First-principles calculations of the structural, dynamical, and electronic properties of liquid MgO

Bijaya B. Karki,[1] Dipesh Bhattarai,[1] and Lars Stixrude[2,*]
[1]*Department of Computer Science, and Department of Geology and Geophysics, Louisiana State University, Baton Rouge, Louisiana 70803, USA*
[2]*Department of Earth and Planetary Sciences, University of California, Berkeley, California, 94720, USA*
(Received 18 August 2005; revised manuscript received 13 January 2006; published 12 May 2006)

The structural, dynamical, and electronic properties of liquid MgO have been investigated over a wide range of pressure (0 to ~240 GPa) and temperature (3000–10 000 K) using first-principles molecular dynamics (FPMD) within the framework of density-functional theory and the pseudopotential approximation. Our results show that the liquid structure is highly sensitive to compression: the Mg-O coordination number increases from 5 at zero pressure to 7 at high pressure. The Grüneisen parameter and heat capacity are found to increase upon twofold compression by 40% and 20%, respectively. The dynamical behavior of the liquid phase is characterized by the diffusion coefficient, which is found to decrease with increasing pressure and to increase with increasing temperature in a way that can be accurately characterized by an Arrhenius relationship with activation energy and volume of 0.85 eV and 1.3 $Å^3$, respectively. The calculated electronic density of states show that the electronic structure of the liquid phase differs substantially from that of the crystalline phase: the liquid has no band gap and a density of states at the Fermi level increases with increasing volume and temperature.

DOI: 10.1103/PhysRevB.73.174208 PACS number(s): 61.20.Ja, 65.20.+w, 91.60.−x

I. INTRODUCTION

Understanding the behavior of the liquid state of oxides such as MgO at high pressure is important for several reasons. First, Mg and O are thought to be the two most abundant elements in Earth's mantle. Knowledge of the physical properties of liquid MgO under extreme pressure and temperature conditions of the deep interior is essential to modeling the thermal, chemical, and dynamical state of the Earth. For instance, the equation of state of the liquid is an important factor controlling the relative density of partial melts produced by geological processes and coexisting solids, and thus whether these melts will rise or sink.[1] The diffusivity controls the rate of chemical reaction of liquids with their surroundings, and can be related to the viscosity, which controls the rate of transport. Second, MgO is a prototype oxide and a simple system with a wide stability field: understanding the physics of this liquid is expected to lend considerable insight into the behavior of other oxide and silicate liquids. Third, relevant experimental studies are still lacking so the computational approach will help better characterize the liquid state thermodynamic and elastic properties at high pressure.

Molecular dynamics (MD) simulations based on semiempirical or *ab initio* models[2–9] were previously employed extensively to investigate both crystalline and liquid phases of the mantle materials. First-principles molecular dynamics (FPMD) simulations have just begun to appear for the majority of Earth minerals including MgO (Ref. 10) and $MgSiO_3$ (Ref. 11). Quantitative predictions are now feasible because the FPMD simulations involving several tens to a few hundreds of atoms for durations of several picoseconds can be performed with moderate computing resources. While melting of MgO was the focus of a recent first-principles study,[10] the structural, dynamic, and electronic properties of the liquid state are yet to be studied. The FPMD approach can be considered as an attractive complement to experiment because experimental measurements, particularly at extreme pressure-temperature conditions, are difficult to conduct. For instance, the only experimental data relevant to the high-pressure liquid phase are a study of melting of MgO up to 32 GPa (Ref. 12).

In this paper, we report a detailed FPMD investigation of the liquid state of MgO as a function of pressure and temperature. We calculate and analyze the structural, dynamical, and electronic properties. The organization of the paper is as follows: Sec. II presents the FPMD technique used and other computational details. Section III presents the calculated results with discussion of the equation of state, thermodynamic properties, geometric and electronic structures, and dynamical properties. Section IV draws some conclusions.

II. METHODOLOGY

The computations have been performed using the first-principles molecular dynamics method. The key difference between FPMD and traditional molecular dynamics simulations is that the interatomic forces in FPMD are calculated using density-functional theory[13] within the local density approximation (LDA)[14] and plane-wave pseudopotental theory. Once the electronic structure of a given atomic system is determined, the required interatomic forces are computed from the Hellmann–Feynman theorem. One thus performs Born–Oppenheimer molecular dynamics simulations, i.e., the interatomic forces are computed at each time step of the simulation from a fully self-consistent solution of the electronic structure problem.[15] We have found that the electronic structure of the liquid, which is described in detail below, is not that of an insulator. We have therefore used the finite temperature formulation of density-functional theory.[16] We

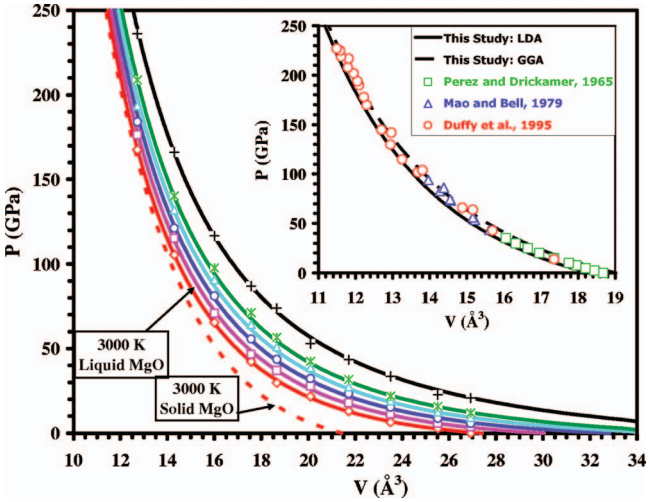

FIG. 1. (Color) Equation of state of liquid MgO at 3000 (diamonds), 4000 (squares), 5000 (circles), 6000 (triangles), 7000 (asterisks), and 10 000 K (crosses). The uncertainties are within the size of the symbols used to represent the data. The FPMD results are fit to the Mie-Grüneisen equation of state [lines, Eq. (3)] with the parameter of the reference isotherm at 3000 K as given in the text, and the thermal pressure described by: $P_{\mathrm{TH}}(V,T)=A(V)/V(T-T_0)$ with $A(V)/6K=0.93-1.25(V-V_0)/V_0$. The inset shows the equation of state for the static lattice (LDA and GGA results represented by the solid and dashed lines, respectively), compared with the room-temperature experimental data (Refs. 20–22).

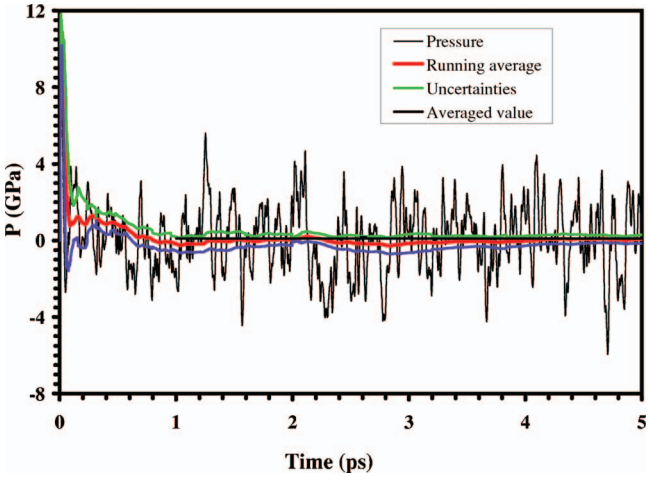

FIG. 2. (Color) Pressure as a function of time over 5 ps period of simulation. Also shown are the running time average, uncertainties, and the averaged value taken over the time period of last 4 ps.

have used ultrasoft Mg (with the core radius of 1.06 Å and the $3s^2$ electronic configuration) and O (with the core radius of 0.8 Å and the $2s^22p^4$ electronic configuration) pseudopotentials and the VASP parallel code.[16] We have used a plane-wave cutoff of 400 eV and gamma point sampling[17] for both the solid and liquid phases. The Pulay correction, which varies with compression from 2.3 to 4.2 GPa over the volume range considered in this study, has been added to the calculated total pressure.[18] The effect of the generalized gradient corrections (GGA) (Ref. 19) is shown to systematically overestimate the volume by about 2%, compared to the LDA result throughout the pressure range considered (see Fig. 1, inset). The calculated equation of state for the static lattice with LDA compares extremely well with experimental data[20–22] over a wide range of pressure since the zero-point and room-temperature contributions would increase the volume by about 2% (Ref. 23). The predicted differences between LDA and GGA volumes are consistent with previous theoretical calculations that used essentially the identical electronic structure method,[10] which also showed that the LDA melting temperature of MgO at zero pressure agrees much better with the experimental value than the GGA melting temperature.[12]

Our FPMD approach uses the canonical (*NVT*) ensemble in which the number of atoms in the periodically repeated unit cell (N), the volume (V), and the temperature (T) are fixed. Temperature is controlled using an extended Lagrangian formulation in which a degree of freedom is included to represent a reservoir (thermostat).[24] The Lagrangian is

$$L=\frac{1}{2}\sum_i m_i|v_i|^2-V(\vec{r}_i)+\frac{1}{2}Q\dot{s}^2-(f+1)k_BT_0\ln s, \quad (1)$$

where s is the new dynamical variable and Q is the associated mass parameter. T_0 is the externally set temperature and f is the number of degrees of freedom in the system. To speed convergence, Q is chosen so that the period of oscillation of the temperature (or s) is similar to the mean period of atomic vibrations. Our *NVT* ensemble consists of 64 atoms in a cubic supercell. The crystalline structure is first melted and equilibrated at 10 000 K for a period of 5 ps. We then quench the system from 10 000 K to a desired lower temperature of 7000 K over a time interval of 2 ps. At this temperature, we first thermalize the system for 1 ps and collect data over another 4 ps. The same procedure is repeated for subsequent lower temperatures. At each temperature, we confirm that the system is in the liquid state by analysis of the radial distribution function and the mean-square displacement (MSD) as a function of time. Figure 2 shows that the running time average of the total pressure (with Pulay correction included) for the liquid phase at 3000 K converges very well over the period of 5 ps. Note that a time step of 1 fs is used. Microcanonical simulations show that the systematic drift in the total energy is less than 0.0002 and 0.0005 eV/MgO over the period of 5 ps at 3000 and 10 000 K, respectively. Uncertainties in the energy and pressure were computed by the blocking method.[25] The convergence of the time-averaged properties has been confirmed by extending the run duration up to 10 ps. Simulations with a larger system of 216 atoms also did not produce significantly different results.

We have performed FPMD simulations of the liquid state at ten volumes $V/V_0=0.982$, 0.931, 0.858, 0.793, 0.752, 0.681, 0.641, 0.584, 0.522, and 0.465, where $V_0=27.40$ Å^3 is the zero pressure volume at 3000 K (see Sec. III B). The corresponding GGA value of V_0 is 28.27 Å^3, which is overestimated relative to the LDA volume as in the case of the static lattice. Computations are performed along six iso-

therms: 3000, 4000, 5000, 6000, 7000, and 10 000 K, that are expected to encompass the melting transition over the pressure range investigated. For comparison, experimental determinations of the zero pressure melting temperature are 3040±100 K (Ref. 12) and 3250±20 K (Ref. 26). Computations based on density-functional theory in the local density approximation find that the melting temperature increases from 3070±50 K at zero pressure to 8144±40 K at 136 GPa (Ref. 10). Extrapolation of these theoretical results with the Simon equation[27] yields 10 000 K at 220 GPa. We pay particular attention to the variation of liquid state properties along the melting curve computed in Ref. 10 since the electronic structure methods used in that study are essentially identical to ours. We note that an extrapolation of the melting temperature based on experimental measurements[12] to a maximum pressure of 30 GPa, which yield a much lower melting temperature in the Mbar range, has recently been questioned.[8] For comparison, we have also performed FPMD simulations of the crystalline phase along the 3000 K isotherm (Fig. 1).

III. RESULTS AND DISCUSSION

A. Structural properties

The radial distribution function (RDF), $g(r)$, is computed to examine the structural properties of the simulated liquid system.[28,29] The RDF is the probability of finding another atom at a distance r from a specified atom. Taking advantage of the periodicity of the supercell, one can extend the system so that it is possible to calculate the RDF at distances greater than the simulation cell size. We have also computed the partial radial distribution functions $g_{\text{Mg-O}}(r)$, $g_{\text{Mg-Mg}}(r)$, and $g_{\text{O-O}}(r)$. Figure 3 shows the partial RDF at three different compression and temperature conditions along the LDA melting curve. The RDF shows large fluctuations at small distances and approaches unity at larger distances indicating the short-range order and long-range disorder characteristic of the liquid state. The first peaks in the unlike and like partial RDF decrease in amplitude and become broader with compression, consistent with previous calculations.[2,8] The position of the first peak for $g_{\text{Mg-O}}(r)$ systematically shifts to a smaller distance as the compression increases [Fig. 3(a)]. The line shapes for $g_{\text{Mg-Mg}}(r)$ and $g_{\text{O-O}}(r)$ are essentially identical. We also note large differences between liquid and solid pair-correlation functions: The solid phase shows several well-defined peaks after the first peak (Fig. 3).

We estimate the Mg-O coordination number in the liquid by

$$C_{\alpha\beta} = 4\pi\rho x_\beta \int_0^{r_{\min}} r^2 g_{\alpha\beta}(r) dr. \quad (2)$$

Here, ρ is the number density and x_β is the concentration (N_β/N) of species β. Since we are interested only in the nearest neighbors, the cutoff is taken to be the first minimum ($r_{\min}$) of the corresponding partial pair distribution function. The calculated average Mg-O coordination number is 4.5–5 at zero pressure, which is smaller than the crystalline coordination of 6. This agrees with previous calculations.[2,8] The coordination number increases with increasing pressure and exceeds 7 at pressures above 150 GPa (Fig. 4). A similar trend was obtained previously,[2] although in that study, the coordination number remained close to 6 at the high pressure. Our results do not predict any systematic dependence of the coordination number on temperature at constant volume. A large pressure-induced increase in the coordination number was also found in our simulations of $MgSiO_3$ liquid.[11]

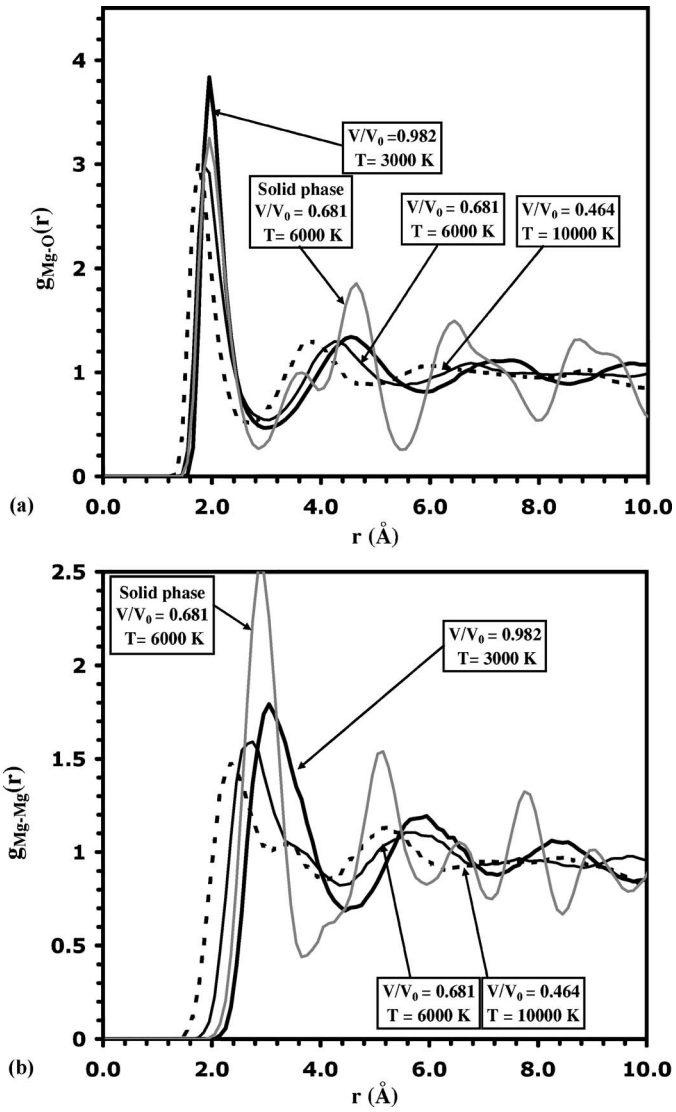

FIG. 3. Radial distribution functions of liquid MgO: (a) Mg-O and (b) Mg-Mg (which is very similar to O-O case) at three different conditions: V/V_0=0.982, T=3000 K (thick lines), V/V_0 =0.681, T=6000 K thin lines), and V/V_0=0.464, T=10 000 K (dashed lines), where V_0=27.40 Å^3. Also shown are the results for solid MgO at V/V_0=0.681 and 6000 K (thin gray lines).

B. Equations of state

Our FPMD results (Fig. 1) are described with the Mie-Grüneisen equation of state

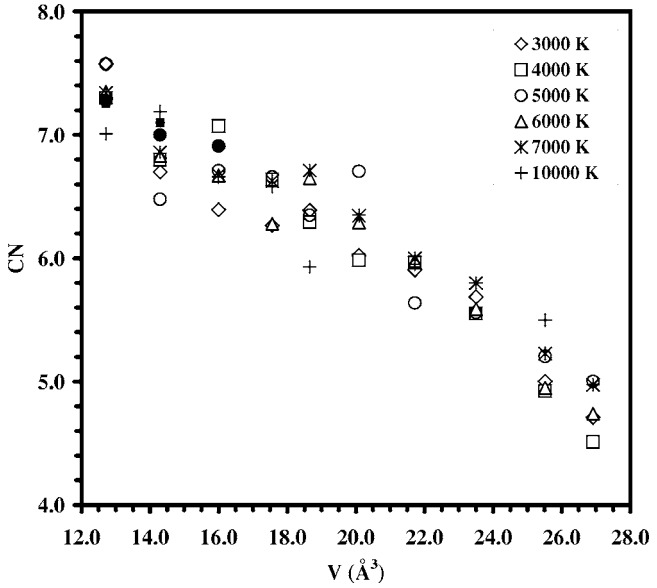

FIG. 4. Mg-O coordination number (CN) of liquid MgO as a function of volume at 3000 (diamonds), 4000 (squares), 5000 (circles), 6000 (triangles), 7000 (asterisks), and 10 000 K (crosses). Also shown are values at 8000 (filled circles) and 9000 K (filled squares) at some compressed volumes.

$$P(V,T) = P(V,T_0) + P_{\mathrm{TH}}(V,T), \tag{3}$$

where $P(V,T_0)$ is the pressure on the reference isotherm, and $T=T_0$ and $P_{\mathrm{TH}}(V,T)$ are the thermal pressure. We find that the thermal pressure is linear in temperature over the entire range of volume and temperature studied (see Fig. 5) (Refs. 30 and 31), including in the supercooled liquid regime that lies below the LDA melting temperature at high pressure. Analysis of the atomic structure also shows continuous trends across the melting line (previous section). The isotherms diverge on compression; that is, the thermal pressure increases on compression. The reference isotherm, taken to be $T_0=3000$ K, is accurately described by the third-order Birch–Murnaghan equation of state with zero pressure volume, bulk modulus, and first pressure derivative of the bulk modulus: $V_0=27.40$ (±0.25) Å^3, $K_0=30.76$ (±2.9) GPa, and $K_0'=5.03$ (±0.33). For comparison, the equation of state parameters obtained from the potential-induced breathing (PIB) model[2] are $V_0=27.0$ Å^3, $K_0=59.2$ GPa, and $K_0'=3.83$.

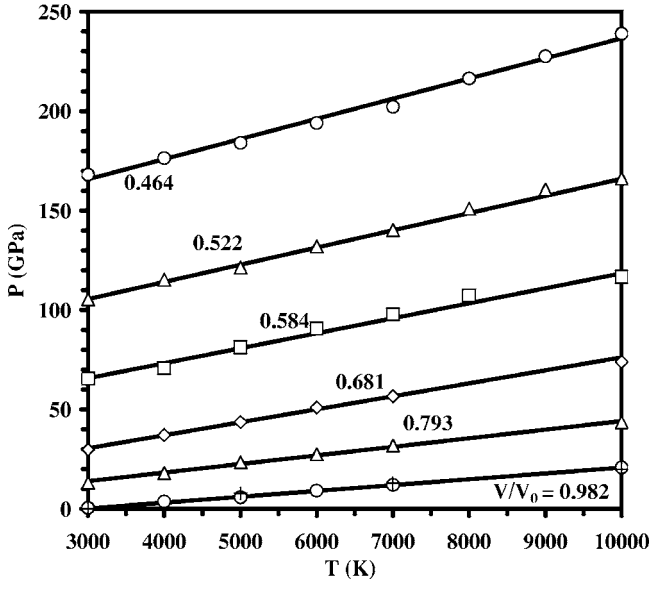

FIG. 5. The total pressure at six different volumes, $V/V_0=0.982$, 0.793, 0.681, 0.584, 0.522, and 0.464. Also shown are results (crosses) of a 216-atom simulation at $V/V_0=0.982$, where $V_0=27.40$ Å^3. The uncertainties are within the size of the symbols used to represent the data.

The equation of state of the solid phase at 3000 K is also shown in Fig. 1 for comparison. The difference in the zero pressure volume of the solid and liquid phase at 3000 K is 5.79 Å^3/MgO, which is comparable to the volume change on melting of ~4.6 to ~6.2 Å^3 from previous calculations.[2–5,10] With increasing compression, the volume difference between the solid and liquid phase drops rapidly, reaching 0.15 Å^3 at 150 GPa, and it appears to asymptotically approach zero. A very similar trend was previously predicted.[2]

We have also calculated the thermal Gruneisen parameter, defined as $\gamma=(V/C_V)(\partial P_{TH}/\partial T)$, where $C_V=\partial E/\partial T$ is the heat capacity at constant volume. A linear equation is fit to the calculated energy-temperature results at each volume to derive C_V. Both γ and C_V increase with increasing compression [Figs. 6(a) and 6(b)]. The behavior of the liquid is in marked contrast to the crystalline phase for which C_V remains nearly unchanged with compression and γ decreases with compression.[23] At high pressure the heat capacity of the liquid substantially exceeds the Dulong–Petit limit that is closely obeyed by the crystalline phase. We attribute the larger heat capacity of the liquid to the change in structure of the liquid with increasing temperature. Whereas the mean coordination number is insensitive to temperature at constant volume, the range of coordination environments increases with increasing temperature. We attribute the increase of γ with compression to the pressure-induced change in the structure of the liquid: higher coordination numbers are expected to result in larger values of the Grüneisen parameter according to the analysis of Ref. 32. Our recent study of $MgSiO_3$ liquid shows many similarities:[11] the value of C_V also substantially exceeds the Dulong–Petit value, although in the case of the silicate C_V decreases slightly with compression. In the silicate, the Grüneisen parameter also increases on compression, although much more rapidly than in the case of MgO.

C. Dynamical properties

Diffusion is an important dynamical phenomenon for a liquid phase. It can be characterized by calculating diffusion coefficient[33] as follows:

$$D = \lim_{t\to\infty} \frac{\langle [r(t)]^2 \rangle}{6t}, \tag{4}$$

where

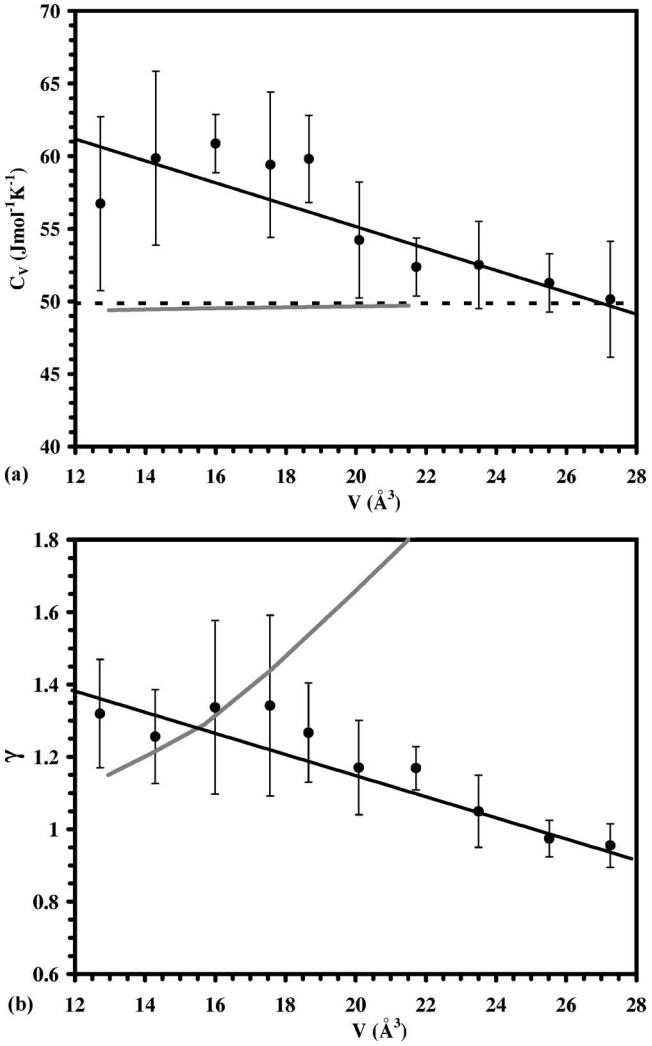

FIG. 6. Isochoric heat capacity, C_V (a) and thermal Gruneisen parameter, γ of liquid MgO (b) as a function of volume. The gray line represents the quasiharmonic lattice-dynamics result for the solid phase at 3000 K from Ref. 23. The dashed line is Dulong–Petit limit.

$$\langle [r(t)]^2 \rangle = \frac{1}{N} \sum_{i=1}^{N} |\vec{r}_i(t+t_0) - \vec{r}_i(t_0)|^2 \tag{5}$$

is the mean-square displacement, and $\vec{r}_i(t_0)$ and $\vec{r}_i(t+t_0)$ are the positions of ith atom at the start and end of the time interval t. The MSD for a given time t is then calculated by averaging over time origins (t_0) (Ref. 28). In our calculations, we account for the translational symmetry of the system so that the MSD value is not restricted by the size of the supercell. The calculated MSD as a function of time at three different conditions along the LDA melting curve is shown in Fig. 7(a). It is clear that the MSD is linear with time. The calculated total self-diffusion coefficients are fit to the Arrhenius relation [Fig. 7(b)],

$$D(P,T) = D_0 \exp[-(E_a + PV_a)/RT], \tag{6}$$

with D_0=200 m^2/s, E_a=0.85 eV the activation energy, and V_a=1.3 Å^3 the activation volume. The diffusion constant can

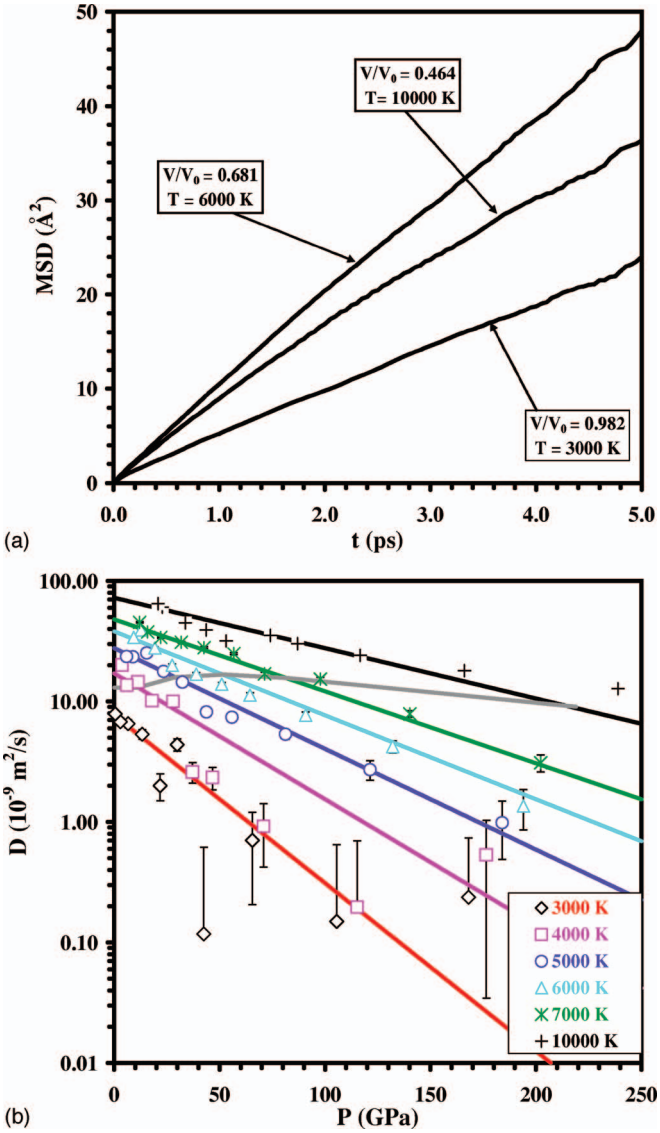

FIG. 7. (Color) (a) Time dependence of the mean-square displacement (MSD) in liquid MgO at three points along the LDA melting curve. (b) The calculated diffusion coefficient as a function of pressure and temperature, and the fit (lines) to the Arrhenius law. The symbols have the same meanings as in Fig. 1. The thick solid line represents the value along the LDA melting curve.

also be obtained for each atom type individually. The calculated values of the diffusion constant at different pressures and temperatures for the O atoms are 10%–15% larger than the total values whereas those for the Mg atoms are 8%–12% smaller than the total value. The results show that temperature systematically enhances diffusion whereas pressure systematically suppresses it. The result of these competing effects is that the diffusion coefficient is nearly constant along the LDA melting curve: D varies by only a factor of 2 along the melting curve up to at least 200 GPa.

D. Electronic properties

The electronic density of states (DoS) is calculated for the solid and liquid at three points along the LDA melting curve

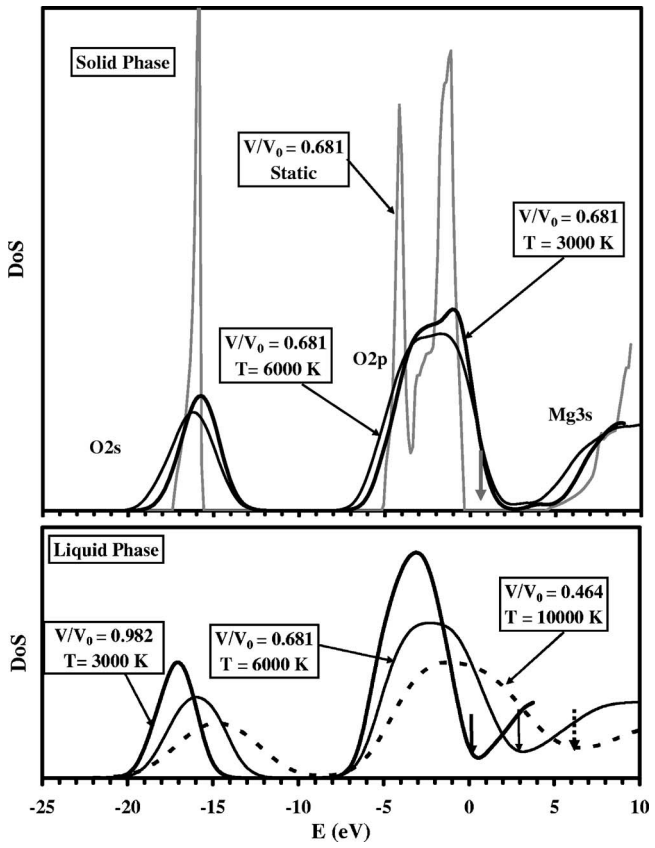

FIG. 8. Electronic density of states of solid MgO (top) at $V/V_0=0.681$ for the static lattice, and from FPDM simulations at 3000 and 6000 K, and of liquid MgO (bottom) at three different V-T conditions along the LDA melting curve. The short vertical arrows indicate the positions of Fermi energy.

(Fig. 8). There is a clear minimum near the Fermi level but no gap in the case of the liquid phase. With increasing pressure, the density of states at the Fermi level decreases and the valence O-2p band begins to split. With increasing temperature, the density of state at the Fermi level increases. The competing influence of pressure and temperature leave the density of states at the Fermi level nearly constant along the LDA melting curve. These features are reminiscent of evolution of the electronic structure of the crystalline phase in which the gap increasingly opens on compression and the valence band shows a similar splitting, with the important difference that in the static crystal a well defined and large gap is present over the entire range of the volume explored here.[34,35] The local density approximation is known to underestimate the band gap, although beyond the scope of this study, it would be interesting to explore the influence of the other forms of the exchange-correlation functional on the predicted band closure.

In crystalline MgO, Mg atoms give up their valence electrons, which along with those from O atoms are primarily localized in the vicinity of O ions, thereby making the oxide highly ionic in the nature.[35,36] As a result, the electronic distribution shows nearly perfect spherical symmetry about each O site. In the liquid phase, due to dynamic rearrangement of atoms, the spherical charge-density distributions

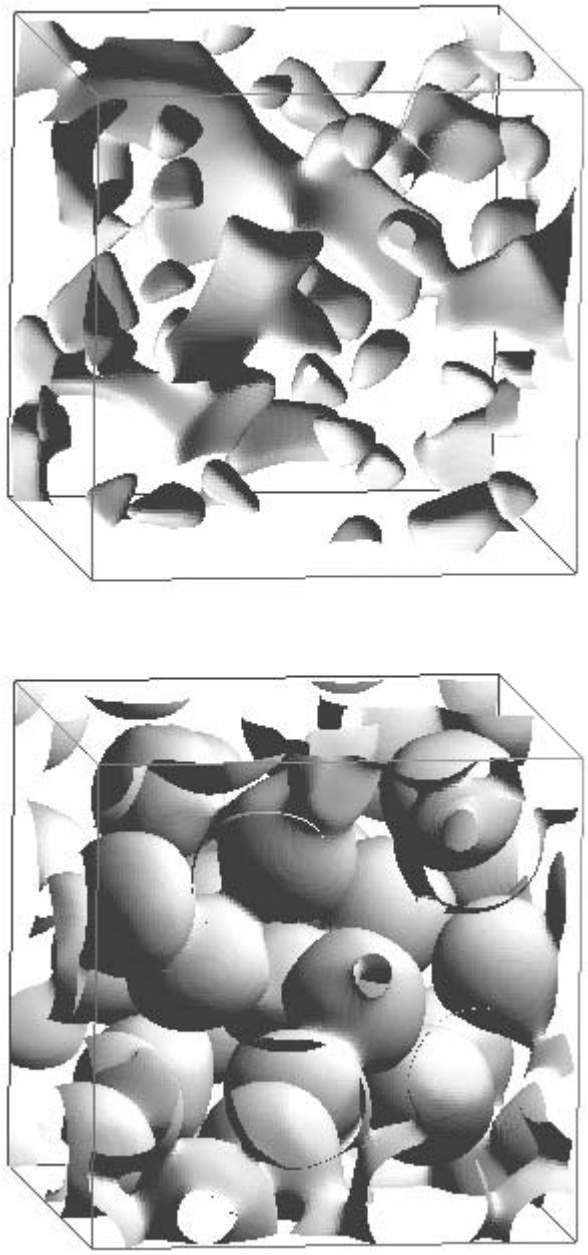

FIG. 9. Isosurfaces at 0.05 (top) and 0.15 Å^{-3} (bottom) of the electron density of liquid MgO at $V/V_0=0.982$ and $T_0=3000$ K.

are significantly perturbed [Fig. 9 (top)]. The electron density isosurfaces form interatomic bridges instead of forming isolated spherical surfaces [Fig. 9 (bottom)]. It is also clear that the ionic nature of interatomic charge transfer remains to be unaffected to a great extent.

IV. CONCLUSIONS

We have successfully applied the first-principle molecular dynamics method within the local density and pseudopotential approximations to explore the structural, dynamic, and electronic properties of liquid MgO, an important com-

ponent of Earth's mantle, over a wide range of pressure (0 to ~240 GPa) and temperature (3000–10 000 K). The calculated energy and thermal pressure are shown to be linear in temperature. The pressure-volume-temperature relationships are well represented with the standard Mie-Grüneisen equation of state. The calculated heat capacity and Grüneisen parameter are shown to increase with compression. The liquid structure is analyzed by calculating the pair-correlation functions and Mg-O coordination number, which vary substantially with compression. For instance, the Mg-O coordination number increases from about 5 at zero pressure to above 7 at high pressure. Finally, our results show that the electronic structure of the liquid state shows some significant features, particularly, band-gap closure and nonspherical valence charge-density distribution about O sites. The liquid state differs substantially from the crystalline state in terms of geometric and electronic structure.

ACKNOWLEDGMENTS

This work was supported by the NSF under Grant No. EAR 0409074. Computing facilities were provided by CCT and BCVC at Louisiana State University.

*On leave from: Department of Geological Sciences, University of Michigan, Ann Arbor, Michigan 48109, USA.

[1] S. M. Rigden, T. J. Ahrens, and E. M. Stolper, Science **226**, 1071 (1984).
[2] R. E. Cohen and Z. Gong, Phys. Rev. B **50**, 12301 (1994).
[3] R. E. Cohen and J. S. Weitz, Geophys. Monogr. **101**, 185 (1998).
[4] L. Vocadlo and G. D. Price, Phys. Chem. Miner. **23**, 42 (1996).
[5] R. E. Cohen and J. S. Weitz, Geophys. Monogr. **101**, 185 (1998).
[6] A. B. Belonoshko and L. S. Dubrovinsky, Am. Mineral. **81**, 303 (1996).
[7] A. Strachan, R. Cagin, and W. A. Goddard III, Phys. Rev. B **63**, 096102 (2001).
[8] A. Aguado and P. A. Madden, Phys. Rev. Lett. **94**, 068501 (2005).
[9] D. Alfe, L. Vocadlo, G. D. Price, and M. J. Gillan, J. Phys.: Condens. Matter **16**, s973 (2004).
[10] D. Alfe, Phys. Rev. Lett. **94**, 235701 (2005).
[11] L. Stixrude and B. B. Karki, Science **310**, 297 (2005).
[12] A. Zerr and R. Boehler, Nature (London) **371**, 506 (1994).
[13] W. Kohn and L. Sham, Phys. Rev. **140**, A1133 (1965); P. Hohenberg and W. Kohn, Phys. Rev. **136**, B864 (1964).
[14] D. M. Ceperley and B. J. Alder, Phys. Rev. Lett. **45**, 566 (1980).
[15] N. D. Mermin, Phys. Rev. **137**, A1441 (1965).
[16] G. Kresse, J. Hafner, and R. J. Needs, J. Phys.: Condens. Matter **4**, 7451 (1992); G. Kresse and J. Furthmuller, Comput. Mater. Sci. **6**, 15 (1996).
[17] H. J. Monkhorst and J. D. Pack, Phys. Rev. B **13**, 5188 (1976).
[18] G. P. Francis and M. C. Payne, J. Phys.: Condens. Matter **2**, 4395 (1990).
[19] Y. Wang and J. P. Perdew, Phys. Rev. B **44**, 13298 (1991).
[20] E. A. Perez-Albuerne and H. G. Drickamer, J. Chem. Phys. **43**, 1381 (1965).
[21] H. K. Mao and P. M. Bell, J. Geophys. Res. **84**, 4533 (1979).
[22] T. S. Duffy, R. J. Hemely, and H. K. Mao, Phys. Rev. Lett. **74**, 1371 (1995).
[23] B. B. Karki, R. M. Wentzcovitch, S. de Gironcoli, and S. Baroni, Phys. Rev. B **61**, 8793 (2000).
[24] S. Nose, J. Chem. Phys. **81**, 511 (1984).
[25] H. Flyvbjerg and H. G. Petersen, J. Chem. Phys. **91**, 461 (1989).
[26] C. Ronchi and M. Scheindlin, J. Appl. Phys. **90**, 3325 (2001).
[27] F. Simon, Trans. Faraday Soc. **33**, 65 (1937).
[28] J. R. Chelikowsky, J. J. Derby1, V. V. Godlevsky, M. Jain, and J. Y. Raty, J. Phys.: Condens. Matter **13**, 817 (2001).
[29] M. J. Allen and D. J. Tildesley, *Computer Simulation of Liquids* (Oxford University Press, Oxford, 1987).
[30] B. B. Karki, Am. Mineral. **85**, 1447 (2000).
[31] O. L. Anderson, J. Phys. Chem. Solids **58**, 335 (1997).
[32] R. Jeanloz and M. M. Roufosse, J. Geophys. Res. **87**, 763 (1982).
[33] R. Virkkunen, K. Laasonen, and R. Nieminen, J. Phys.: Condens. Matter **3**, 7455 (1991).
[34] M. S. T. Bukowinski, J. Geophys. Res. **85**, 285 (1980).
[35] K. J. Chang and M. L. Cohen, Phys. Rev. B **30**, 4774 (1984).
[36] M. J. Mehl, R. E. Cohen, and H. Krakauer, J. Geophys. Res. **93**, 8009 (1988).